Ocular Motor Nerve Development in the Presence and Absence of Extraocular Muscle

Suzanne M. Michalak,[1–5] Mary C. Whitman,[2,6,7] Jong G. Park,[1–3,5,8] Max A. Tischfield,[2,3] Elaine H. Nguyen,[2,6] and Elizabeth C. Engle[1–3,5–7]

[1]Department of Neurology, Boston Children's Hospital, Boston, Massachusetts, United States
[2]F. M. Kirby Neurobiology Center, Boston Children's Hospital, Boston, Massachusetts, United States
[3]Department of Neurology, Harvard Medical School, Boston, Massachusetts, United States
[4]University of North Carolina School of Medicine, Chapel Hill, North Carolina, United States
[5]Howard Hughes Medical Institute, Chevy Chase, Maryland, United States
[6]Department of Ophthalmology, Boston Children's Hospital, Boston, Massachusetts, United States
[7]Department of Ophthalmology, Harvard Medical School, Boston, Massachusetts, United States
[8]Duke University School of Medicine, Durham, North Carolina, United States

Correspondence: Elizabeth C. Engle, Boston Children's Hospital, CLS 14076, 300 Longwood Avenue, Boston, MA 02115, USA; Elizabeth.Engle@childrens.harvard.edu.

SMM, MCW, and JGP contributed equally to the work presented here and should therefore be regarded as equivalent authors.

Submitted: December 9, 2016
Accepted: March 21, 2017

Citation: Michalak SM, Whitman MC, Park JG, Tischfield MA, Nguyen EH, Engle EC. Ocular motor nerve development in the presence and absence of extraocular muscle. *Invest Ophthalmol Vis Sci*. 2017;58:2388–2396. DOI:10.1167/iovs.16-21268

Purpose. To spatially and temporally define ocular motor nerve development in the presence and absence of extraocular muscles (EOMs).

Methods. *Myf5*^{cre} mice, which in the homozygous state lack EOMs, were crossed to an *Isl*^{MN}*:GFP* reporter line to fluorescently label motor neuron cell bodies and axons. Embryonic day (E) 11.5 to E15.5 wild-type and *Myf5*$^{cre/cre}$*:Isl*^{MN}*:GFP* whole mount embryos and dissected orbits were imaged by confocal microscopy to visualize the developing oculomotor, trochlear, and abducens nerves in the presence and absence of EOMs. E11.5 and E18.5 brainstems were serially sectioned and stained for Islet1 to determine the fate of ocular motor neurons.

Results. At E11.5, all three ocular motor nerves in mutant embryos approached the orbit with a trajectory similar to that of wild-type. Subsequently, while wild-type nerves send terminal branches that contact target EOMs in a stereotypical pattern, the *Myf5*$^{cre/cre}$ ocular motor nerves failed to form terminal branches, regressed, and by E18.5 two-thirds of their corresponding motor neurons died. Comparisons between mutant and wild-type embryos revealed novel aspects of trochlear and oculomotor nerve development.

Conclusions. We delineated mouse ocular motor nerve spatial and temporal development in unprecedented detail. Moreover, we found that EOMs are not necessary for initial outgrowth and guidance of ocular motor axons from the brainstem to the orbit but are required for their terminal branching and survival. These data suggest that intermediate targets in the mesenchyme provide cues necessary for appropriate targeting of ocular motor axons to the orbit, while EOM cues are responsible for terminal branching and motor neuron survival.

Keywords: development, ocular motor nerves, extraocular muscle, animal model, oculomotor

Accurate eye movements are critical to visual navigation and rely on proper innervation of the extraocular muscles (EOMs) by three cranial motor nerves. The oculomotor nerve (CN3) inferior division innervates the inferior rectus (IR), medial rectus (MR), and inferior oblique (IO) muscles, while the superior division innervates the superior rectus (SR) and the levator palpebrae superioris (LPS) muscles. The trochlear nerve (CN4) innervates the superior oblique (SO) muscle, and the abducens nerve (CN6) innervates the lateral rectus (LR) muscle and, in mice, the retractor bulbi (RB) muscle (not present in humans). This stereotyped EOM innervation depends on the ability of developing ocular motor axons to correctly exit the brainstem, fasciculate into nerve bundles, traverse the mesenchyme, enter the developing orbit, and contact the appropriate target muscle.

Perturbations in development of the ocular motor nerves can cause paralytic strabismus and ptosis, resulting in syndromes referred to as congenital cranial dysinnervation disorders (CCDDs).[1,2] Genetic studies in humans and functional studies in mice have revealed that CCDDs can arise from failure of cranial motor neuron specification[3–6] or failure of cranial axon growth and guidance.[7–11] Axons may have errors in their trajectory,[9] stall en route to their target EOM,[7,12] or stereotypically innervate the wrong EOM.[6,12] Loss-of-function studies in mouse have implicated Robo/Slit in oculomotor cell body migration[13] and possibly nerve extension,[14] CXCR4 in oculomotor axon exit from the neuroepithelium,[15] neuropilins (receptors for semaphorins) in oculomotor fasciculation,[16–18] and both α2-chimaerin and Eph/ephrin forward and reverse signaling in abducens axon growth and guidance.[12] Studies in chick and zebrafish support a repellent role for semaphorins, an attractive role of CXCL12 and hepatocyte growth factor (HGF), and a regulatory role of α2-chimaerin in oculomotor nerve guidance.[15,19–21] Many of these growth factors and ligands are expressed diffusely in cranial mesenchyme as well as surrounding and within developing EOMs,[12,14,15,19–21] and thus the relative roles of mesenchymal versus EOM-derived cues have not been fully elucidated. Here, we studied

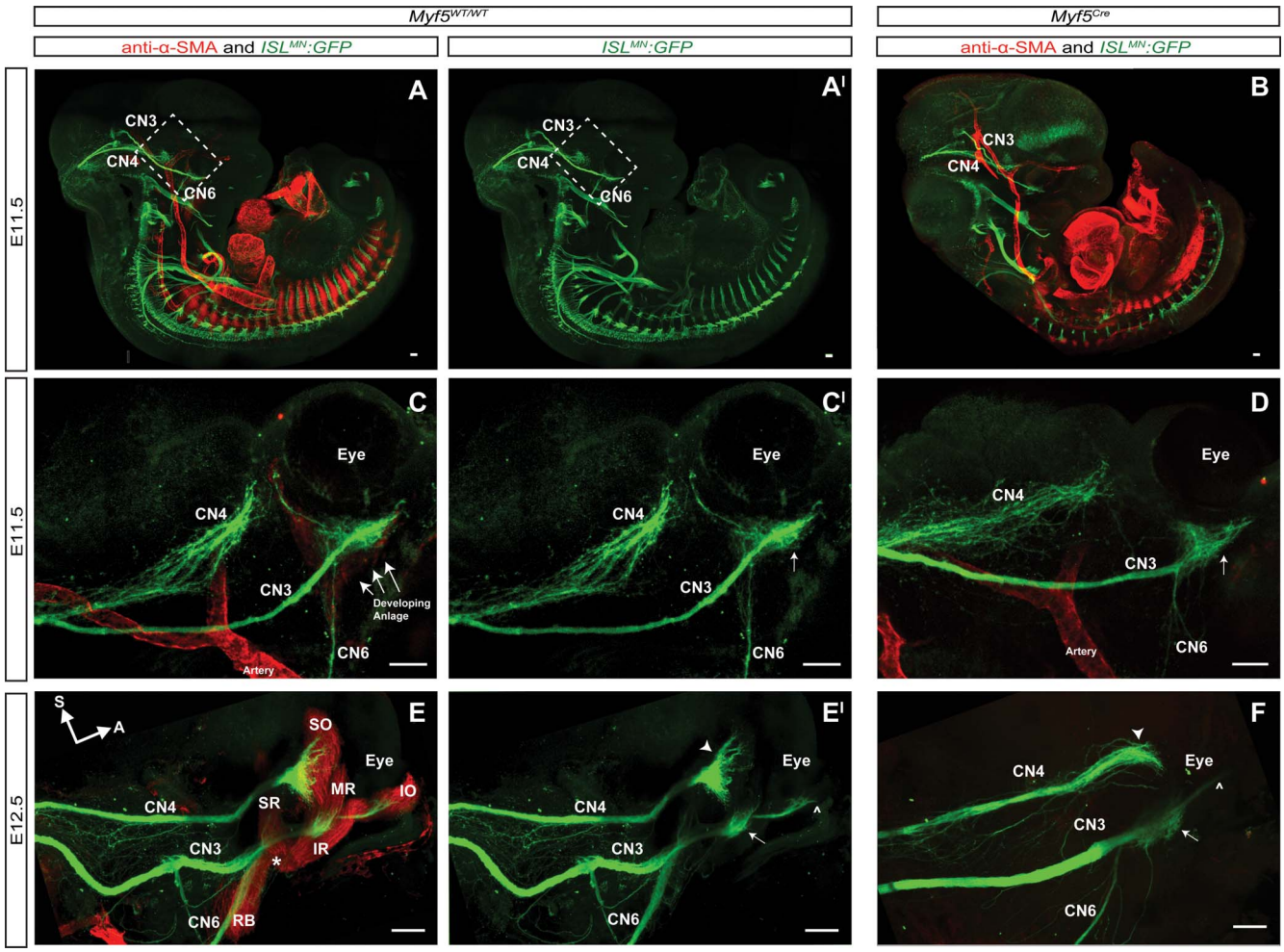

Figure 1. Sagittal views of cranial nerve and extraocular muscle development in E11.5 and E12.5 *Myf5*$^{WT/WT}$*::Isl*^{MN}*:GFP* and *Myf5*^{Cre}*::Isl*^{MN}*:GFP* embryos. Ocular motor nerves are genetically labeled (*green*), and EOM and arteries are antibody labeled with α-SMA (*red*). Extraocular muscles are absent in *Myf5*^{Cre} embryos (**B**, **D**, **F**), and thus the red muscle channel has been turned off in wild-type images (**A**′, **C**′, **E**′), to permit equivalent comparison of nerve trajectories in the presence and absence of EOMs. (**A**, **A**′) Whole mount wild-type embryo and (**B**) whole mount *Myf5*^{Cre} embryo at E11.5. The trajectories of the nerves from the brainstem appear nearly identical in mutant and wild-type embryos at E11.5. The *dotted line* denotes the area of the orbit imaged in greater detail in (**C**), (**C**′), and (**D**). (**C**, **C**′, **D**) Magnified image of whole mounts at E11.5. CN4 is defasciculated, while CN6 is fasciculated along their nerve trunks, and distal CN3 has formed a decision region. The developing muscle anlage stained with α-SMA can be seen in the wild type (**C**), and an artery within the orbit stained with α-SMA is visible in both mutant and wild-type (**C**, **D**). No muscle anlage can be seen in the mutant (**D**). (**E**, **E**′, **F**) Orbital imaging at E12.5. In the *Myf5*$^{WT/WT}$ orbit, distinct extraocular muscles have formed and share a common origin at the annulus of Zinn (**E**, *asterisk*). The trunk of CN4 is now fasciculated, while the distal end forms a decision region adjacent to the SO and sends terminal branches into the body of the muscle (**E**, **E**′, *arrowhead*). By contrast, the distal end of CN4 in the *Myf5*^{Cre} orbit fails to form an equivalent distal decision region and has no terminal branches (**F**, *arrowhead*). In the wild-type orbit, the inferior division decision region has become more compact (**E**′, *long arrow*) and extends a branch to the IO muscle (**E**′, *caret*). The *Myf5*^{Cre} CN3 terminal decision region is less compacted (**F**, *long arrow*) and the branch to the IO muscle appears hypoplastic (**F**, *caret*). *Scale bars*: 100 μm. *Arrow* in the *lower left* corner indicates direction relative to the eye. A, anterior (toward front of eye); S, superior; ISL, islet1; α-SMA, α-smooth muscle actin.

oculomotor, trochlear, and abducens nerve development in mice by using imaging methods that allow examination of nerve trajectories in fine temporal and spatial detail, and we examined the role of EOMs on ocular motor nerve development by comparing wild-type mice to genetically modified mice lacking EOMs.

Methods

Generation of Mice Lacking Extraocular Muscles

Myf5 and Mrf4 (also known as Myf6) are upstream of MyoD in muscle precursor differentiation; alternate Tbx1 and Pax3 pathways can initiate MyoD expression in pharyngeal muscles and in body and limb skeletal muscles, respectively, but not in EOMs.[22,23] Regulatory elements for *Mrf4* reside within the *Myf5* locus, and *Myf5*-targeted alleles have variable EOM hypoplasia depending on the degree of residual *Mrf4* expression, with complete loss of both *Myf5* and *Myf4* resulting in a specific loss of EOMs.[23] We purchased *Myf5*$^{cre/+}$ mice from Jackson Laboratory (B6.129S4-*Myf5*$^{tm3(cre)Sor}$/J, stock No. 007893; Bar Harbor, ME, USA).[24] This *Myf5*^{cre} strain expresses cre recombinase at the endogenous *Myf5* locus, disrupting the *Myf5* basic helix-loop-helix domain, and is also predicted to disrupt transcription of the adjacent *Mrf4* gene because the *Myf5*^{nlacZ} strain, created by using a similar targeting vector, disrupts expression of both genes and lacks EOMs (but not other muscle types).[25]

Myf5$^{cre/+}$ mice were crossed to transgenic *ISL*^{MN}*:GFP* reporter mice (MGI: J:132726; gift of Sam Pfaff, Salk Institute, San Diego, CA, USA), which contain a farnesylated green

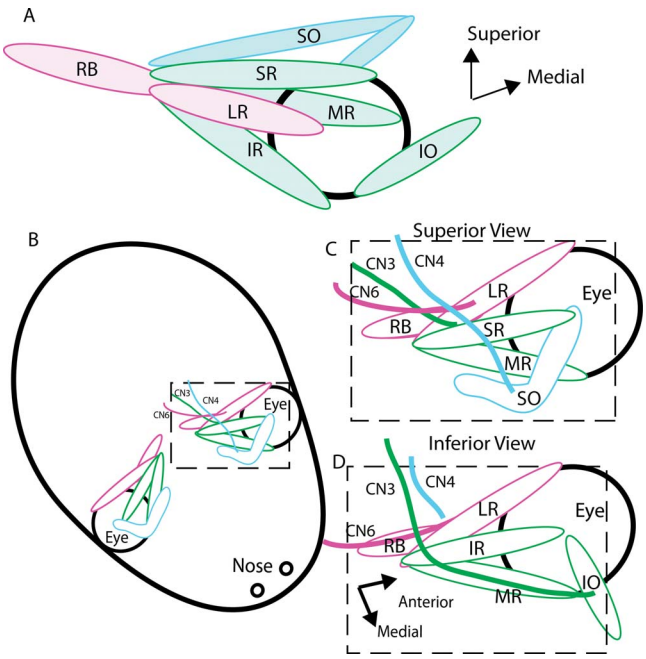

Figure 2. Schematic diagrams of orbital anatomy. (**A**) Schematic diagram showing semisagittal lateral view of mature mouse eye and orbital muscles. (**B**) Horizontal top-down view showing orientation of mature mouse orbits relative to the head; this orientation shifts during early development. (**C**) Schematic of *boxed area* in (**B**), showing the muscles and nerves visible in a top-down, superior view. (**D**) Schematic showing the muscles and nerves visible in a bottom-up, inferior view. The views in (**C**) and (**D**) are those used in Figure 3. Color coding: CN3 and the muscles it innervates (MR, IR, SO, IO) are *green*, CN4 and the muscle it innervates (SO) are *blue*, and CN6 and the muscles it innervates (LR and RB) are *pink*.

fluorescent protein (GFP) that localizes to the membrane of motor neurons and axons and allows for visualization of the nerves during development.[26] ISL^{MN}*:GFP* specifically labels motor neurons and is not cytotoxic. We generated embryos from timed matings of $Myf5^{cre/+}$*::*ISL^{MN}*:GFP* × $Myf5^{cre/+}$ mice. We refer to $Myf5^{+/+}$*::*ISL^{MN}*:GFP* embryos as wild type and $Myf5^{cre/cre}$*::*ISL^{MN}*:GFP* embryos as $Myf5^{cre}$. All animal work was approved and performed in compliance with Boston Children's Hospital Institutional Animal Care and Use Committee protocols and the ARVO Statement for the Use of Animals in Ophthalmic and Vision Research.

Whole Mount Preparation and Imaging

Wild-type and $Myf5^{cre}$ embryos were taken at embryonic day (E) 11.5 and fixed in 4% paraformaldehyde (PFA) overnight (O/N), washed, dehydrated, and placed in Dent's fixative (20% DMSO, 80% methanol) O/N, rehydrated, and placed in blocking solution (5% heat-inactivated goat serum, 20% DMSO, 75% 1× PBS) O/N. Whole mounts were then incubated with anti–actin α-smooth muscle-Cy3 antibody (anti–α-SMA; Sigma-Aldrich Corp., St. Louis, MO, USA) and anti-GFP (Invitrogen, Carlsbad, CA, USA) for 5 days at room temperature (RT), washed, incubated in secondary antibody (488 goat anti-rabbit IgG; Alexa Fluor, Life Technologies, Carlsbad, CA, USA) for 3 days at RT, washed, dehydrated, and cleared O/N in BABB (one part benzyl alcohol and two parts benzyl benzoate). Images were acquired with a Zeiss LSM 710 laser scanning confocal microscope and Zen software (Zeiss, Oberkochen, Germany) and processed with Imaris software (Bitplane, Zurich, Switzerland). $N \geq 3$ were examined for each experiment.

Orbital Dissections and Imaging

From E12.5 onward, orbital dissections provide superior image detail and quality as compared to whole mount preparations. Wild-type and $Myf5^{cre}$ embryos were taken at the appropriate age and fixed in 4% PFA O/N. Cortex and olfactory bulbs above the orbit were removed under a dissecting microscope, leaving the distal cranial nerves and EOMs (if present) intact. Orbits were incubated with anti–α-SMA for 3 days at RT or 4°C, washed, and incubated in secondary antibody for 3 days at RT. After washing with PBS, orbits were further dissected sagitally at E12.5 or, from E13.5 onward, either from the superior aspect, looking down on the orbit from above (superior view), or from the inferior aspect, looking up at the orbit from the palate (inferior view). Tissue was mounted in 70% glycerol and 1% 1M KOH in PBS. Images were acquired and processed as above. $N \geq 3$ were examined for each condition.

Oculomotor Nerve Measurements

Raw images were analyzed with Zen software. The oculomotor nerve was measured at its widest diameter, which occurs where the superior division of CN3 forms in control embryos, adjacent to where CN4 crosses above CN3. The length of the CN3 branch to the IO muscle was measured along its trajectory from the distal decision region to the distal nerve tip. All measurements were taken in three dimensions through z-stacks of 3 μm. Statistical analyses of significance were performed by using unpaired *t*-tests in GraphPad Prism (Graph Pad, San Diego, CA, USA).

Motor Neuron Cell Counts

Litters were taken at E11.5 or E18.5. As $Myf5^{cre}$ mice die at birth, E18.5 was the latest age examined. Whole embryos (E11.5) or brain and brainstem (E18.5) were fixed in 4% PFA O/N, washed in PBS, equilibrated in 30% sucrose, and frozen in optimal cutting temperature (OCT) media. Serial coronal sections of 20-μM thickness were cut on a cryostat and stained with rabbit anti-Islet1 (Isl1; Abcam, Cambridge, MA, USA). After blinding as to genotype, Isl-positive motor neuron nuclei were counted in every fifth section through the rostral-caudal extent of the oculomotor and trochlear nuclei by using the Cell-Counter plug-in in Fiji, and the total number of motor neurons counted was then multiplied by 5. Wild-type and heterozygous mice served as controls. Unpaired *t*-tests were performed in GraphPad Prism. There were $N = 3$ mutant and $N = 3$ control embryos at each of the two ages.

Results

EOMs Are Absent in $Myf5^{cre}$ Embryos

In whole mount views of E11.5 wild-type embryos, the EOM anlage can be seen adjacent to the globe (Figs. 1A, 1C) and by E12.5 the EOM anlage has separated into distinct muscles (Figs. 1E, 1E′). In contrast, homozygous $Myf5^{cre}$ embryos lack EOMs but develop facial and skeletal muscles (Figs. 1B, 1D). Heterozygous $Myf5^{cre/+}$ embryos have normal-appearing EOMs (not shown).

EOMs Are Not Necessary for Initial Pathfinding of Ocular Motor Axons to the Orbit

In E11.5 wild-type embryos, the ocular motor nerves follow stereotypical trajectories to reach the developing orbit (Figs. 1A, 1C). CN4 is defasciculated along its trajectory, while CN6 is fasciculated. The main trunk of CN3 is fasciculated, and its

Investigative Ophthalmology & Visual Science

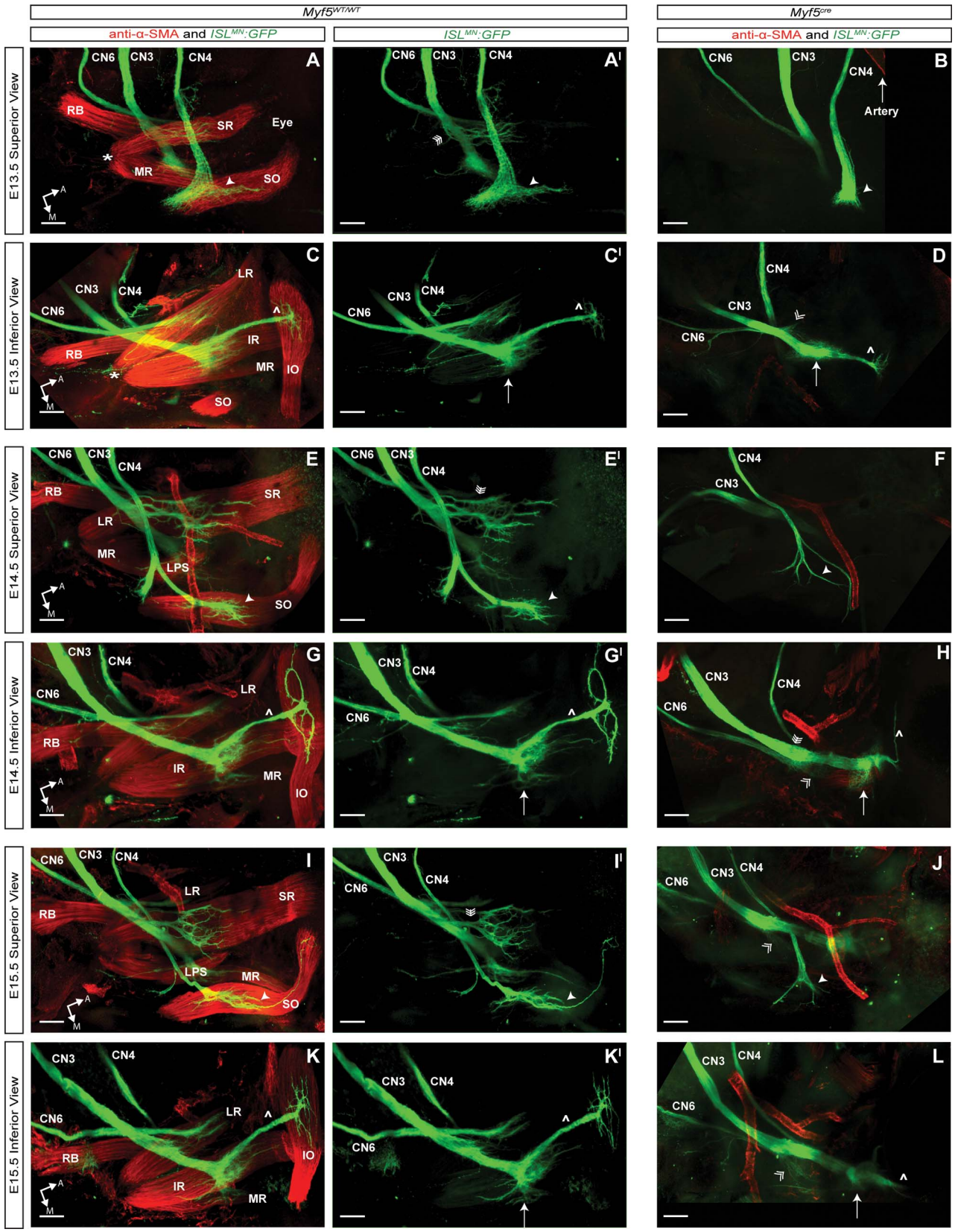

Figure 3. Orbital dissections of E13.5 to E15.5 *Myf5*$^{WT/WT}$*:Isl*^{MN}*:GFP* and *Myf5*^{Cre}*:Isl*^{MN}*:GFP* embryos. Nerves and muscles are labeled and columns arranged as in Figure 1. Orbits are imaged from a superior (**A**, **A′**, **B**, **E**, **E′**, **F**, **I**, **I′**, **J**) or inferior (**C**, **C′**, **D**, **G**, **G′**, **H**, **K**, **K′**, **L**) view, as per Figures 2B through 2D schematics. (**A–D**) At E13.5, *Myf5*$^{WT/WT}$ EOMs share a common origin at the annulus of Zinn (**A**, *asterisk*; **C**). From the superior view (**A**, **A′**) the SO muscle begins to curve at its insertion onto the globe, and the rectus muscles have further differentiated from each other. CN3 superior division has multiple branches extending to the SR muscle (**A′**, *triple-headed arrow*). CN6 has crossed inferiorly to CN3 and extends terminal branches into the LR muscle. From the inferior view (**C**, **C′**), CN3 inferior division sends terminal branches to the IR and MR muscles (**C′**, *long*

Investigative Ophthalmology & Visual Science

arrow), and a well-formed branch to the IO muscle (**C′**, *caret*). At E13.5, the *Myf5*^{Cre} orbit is devoid of EOMs (**B**, **D**). From the superior view (**B**), CN4 has fasciculated but lacks an extensive distal decision region and terminal branches (*arrowhead*), and CN3 superior division is not visible. From the inferior view (**D**), CN3 distal decision region (**D**, *long arrow*) and the branch to the IO muscle (**D**, *caret*) are hypoplastic and misoriented, and CN6 is stunted and barely crosses over CN3 (**D**, *double-headed arrow*). (**E–H**) At E14.5, the *Myf5*$^{WT/WT}$ EOMs continue to grow and change in orientation (**E**, **G**): the SR muscle is now a broad band inserting on the top of the globe, the LPS muscle has appeared between the SR and SO muscles, and the SO muscle has obtained its stereotypic curved shape. There is extensive terminal branching of CN3 superior division into the SR muscle (**E**, **E′**), and CN4 has developed a blunt-ended branch that is not in association with an EOM (**E**, **E′**). CN3 inferior division branch has continued extending terminal branches to the MR and IR muscles, and the branch to the IO muscle extends into the muscle (**G**, **G′**). In the absence of EOM, the *Myf5*^{Cre} CN4 appears thin and has developed multiple aberrant branches (**F**), CN3 main trunk widens (**H**) where the absent superior branch should have formed (**H**, *triple arrowhead*), the inferior division decision region is small, with no visible branches to the IR and MR muscles, and the branch to the IO muscle is now hypoplastic and aberrant (**H**). CN6 trajectory is aberrantly parallel to CN3 and its growth cones pathologically wander (**H**, *double arrowhead*). (**I–L**) At E15.5, *Myf5*$^{WT/WT}$ orbits reveal the near-final ocular motor innervation patterns, and each nerve sends terminal and intramuscular branches into the appropriate EOM. CN3 superior division branches have coalesced into a single trunk, and the blunted branch of CN4 is retracting (**I**, **I′**, **K**, **K′**). By contrast, in *Myf5*^{Cre} orbits the nerves have failed to develop further since E14.5 and appear to be regressing, while the abducens nerve wanders (*double arrowhead*). Although more of the oculomotor nerve appears visible in Figure 2J than in Figure 2F, this is a staining and imaging artifact. In both images, the oculomotor nerve can be seen traveling inferiorly to the trochlear nerve and descending out of view near the stained artery; the embryo in (**J**) was imaged slightly deeper. *Arrows* in the *lower left* corner indicate direction relative to the eye. *Scale bars*: 100 μm.

distal end has formed a decision region (Figs. 1C, 1C′). Despite the absence of the EOM anlage in the E11.5 *Myf5*^{cre} embryos, the ocular motor nerves appear similar to wild-type (Figs. 1B, 1D).

Axons of Ocular Motor Nerves Follow a Stereotypical Spatial and Temporal Trajectory in the Orbit in Both Wild-type and *Myf5*^{cre} Embryos

By E12.5, distinct EOMs are recognizable (Figs. 1E, 1E′); the four rectus muscles and the SO muscle (whose tendon travels through the trochlea before forming its muscle body) share a common origin at the annulus of Zinn (denoted by an asterisk in Fig. 1E), while the IO muscle is located nearer the front of the orbit (see Fig. 2A, schematic). The main trunk of CN4 is now fasciculated, and terminal axons are fanning out into the SO muscle. The CN3 inferior division decision region is nestled adjacent to the MR and IR muscles, and the fasciculated branch to the IO muscle is extending from or through it. Thin branches extend from the CN3 superior and inferior divisions into the SR, MR, and IR muscles. The distal end of the abducens nerve crosses inferiorly to CN3 and extends toward the LR muscle.

Beginning at E12.5, differences are noted in development of ocular motor nerves in the presence and absence of EOMs (Fig. 1F). In *Myf5*^{cre} embryos, distal CN4 does not form the extensive fan-like terminal branches seen in wild-type embryos. The CN3 inferior division decision region remains large; its appearance is similar to wild-type at E11.5. A branch of CN3 extends toward where the IO muscle should be located, but it appears thinner, straighter, and blunter than in wild-type embryos (Fig. 1F, caret).

Ocular Motor Nerves Fail to Develop Terminal Branches in the Absence of EOMs

In mouse, the orbits are oriented slightly laterally (Fig. 2B), and the position changes slightly as the embryo grows, so further anatomic descriptions are in reference to the eye. By E13.5, orbit growth requires that orbital dissections be performed from either the superior (looking down from above) or inferior view (looking up from below; see schematic Figs. 2C, 2D). In E13.5 wild-type embryos, the EOMs continue to grow and separate. The medial origin of the IO muscle is now evident (Figs. 3A, 3C). The distal aspect of CN4 widens considerably, and terminal branches emanate into the SO muscle from one-half of the decision region, while branches from the other half are oriented away from the muscle (Figs. 3A, 3A′). Multiple branches of the CN3 superior division extend from the main trunk and travel along and into the SR muscle (Fig. 3A′, triple-headed arrow). The CN3 inferior division decision region contains multiple nerve branches extending directly into the IR and MR muscles, while a long fasciculated branch extends to and sends terminal branches into the IO muscle. CN6 crosses inferiorly to CN3, extends along the LR muscle, and sends terminal branches into it (Figs. 3C, 3C′).

By E13.5, *Myf5*^{cre} distal ocular motor nerves are clearly aberrant. CN4 terminates in a single blunt end adjacent to where the SO muscle should be (Fig. 3B, arrowhead). The CN3 superior division has not formed, and the nerve trunk is significantly wider where it should have formed, averaging 62.05 ± 8.17 μm in *Myf5*^{cre} embryos and 35.92 ± 8.43 μm in wild type ($P = 0.0052$) (Figs. 4A, 4B). The CN3 inferior division decision region is small and no terminal branches extend toward the region where the IR and MR should be. The branch extending toward where the IO muscle should be is short, thin, and straight rather than arching as seen in wild-type embryos (Figs. 3D, caret; 4C). CN6 appears thinner and shorter than in wild type and ends bluntly just after passing inferiorly to CN3 (Fig. 3D, double-headed arrow).

By E14.5 in wild-type embryos, CN4 provides terminal innervation to the SO muscle. A second branch oriented away from the SO terminates in a blunt end without visible muscle nearby (Figs. 3E, 3E′). The CN3 superior division branches have grown in length and are running along the body of the SR muscle (Figs. 3E, 3E′). The CN3 inferior division continues to send terminal branches into the MR and IR muscles, and the branch to the IO muscle extends further into the muscle (Figs. 3G, 3G′). CN6 crosses inferiorly to CN3 and extends terminal branches into the LR muscle (Figs. 3G, 3G′).

In E14.5 *Myf5*^{cre} embryos, EOMs remain absent (Figs. 3F, 3H). CN4 is thin and forms multiple aberrant distal nerve branches that appear incorrectly oriented relative to the artery visible within the orbit (Fig. 3F). The CN3 superior division has not formed, and the nerve trunk widens where the superior division normally forms (Figs. 3H, 4B). The CN3 inferior division does not extend branches to the area of the IR or MR muscles. The branch to the IO muscle is only a thin wisp extending toward where the muscle would normally be located (Figs. 3H, 4C). CN6, which had crossed inferiorly to the oculomotor nerve at E13.5, now has an aberrant trajectory parallel to the oculomotor nerve.

At E15.5, the ocular motor nerves in wild-type embryos are close to their mature configuration (Figs. 3I, 3K). The CN4 branch to the SO muscle has defined terminal branches associated with the muscle, while the second blunted branch appears thinner and less developed than at E14.5 (Figs. 3I, 3I′). The CN3 superior division has formed a single fasciculated main trunk and developed more extensive intramuscular nerve

Investigative Ophthalmology & Visual Science

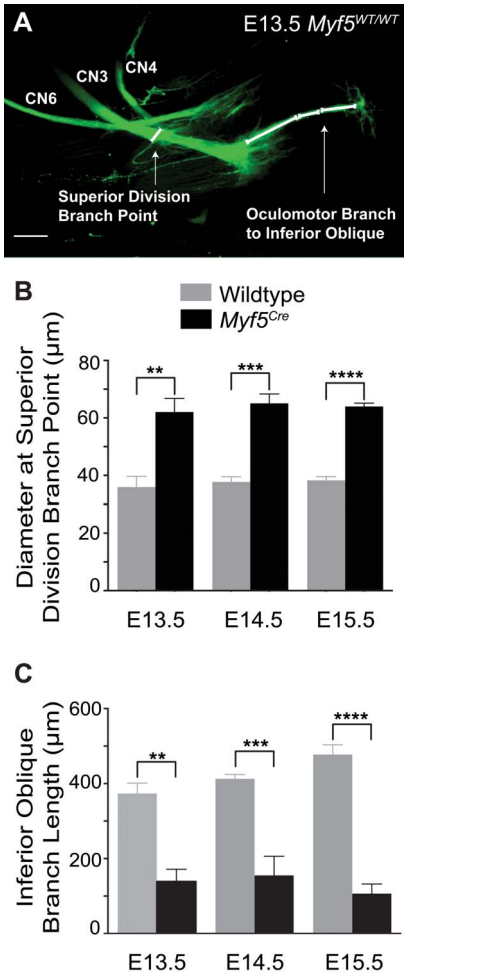

Figure 4. The *Myf5*^{Cre} CN3 widens at the origin of the absent superior division and has a shorter branch to the IO muscle as compared to the *Myf5*$^{WT/WT}$ orbit. (**A**) Orbit of an E13.5 *Myf5*$^{WT/WT}$ from the inferior view as pictured in Figure 2C with measurements illustrated. The diameter of CN3 was measured at the location where the superior division normally forms in control embryos. The length of the inferior division branch to the IO muscle was defined as the distance from the termination of the distal decision region to the distal tip of the nerve and was measured in three dimensions by using two to three straight lines that approximated the curvature of the nerve. (**B**) CN3 superior division branch point is significantly wider in *Myf5*^{Cre} embryos from E13.5 to E15.5 (average from 62.05 ± 8.17 μm at E13.5 to 63.96 ± 2.08 μm at E15.5) than in the wild-type embryos (average 35.92 ± 8.43 μm at E13.5 to 38.26 ± 2.89 μm at E15.5). This difference in width was significant at each age measured (E13.5: $P = 0.0052$; E14.5: $P < 0.0001$; E15.5: $P < 0.0001$). (**C**) At E13.5, CN3 inferior division branch to the IO muscle is significantly longer in *Myf5*$^{WT/WT}$ (373.8 ± 138.7 μm) than in *Myf5*^{Cre} embryos (138.7 ± 56.6 μm; $P = 0.0017$). While this branch continues to lengthen in WT orbits, reaching an average length of 412.8 ± 25.5 μm at E14.5 and 477.6 ± 57.9 μm at E15.5, it fails to lengthen substantially in mutant orbits (155.3 ± 87.7 μm at E14.5 and 106.7 ± 44.0 μm at E15.5). The branch to the IO muscle is significantly shorter in the mutant at each age (E14.5: $P = 0.0007$; E15.5: $P < 0.0001$). *Error bars* represent SEM. WT, wild-type.

branches into the SR (Figs. 3I, 3I′). The CN3 inferior division sends longer terminal branches to the IR and MR muscles, and the IO nerve branch has continued to elongate with its terminal branches in close association with the IO muscle (Figs. 3K, 3K′, 4C). CN6 continues to expand into the LR muscle, and branches to the RB muscle are now visible (Figs. 3K, 3K′).

In E15.5 *Myf5*^{cre} embryos, ocular nerves appear to have started retracting (Figs. 3J, 3L). CN4 maintains a few wandering branches that are mislocalized relative to the normal location of the SO muscle (Fig. 3J). The CN3 trunk where the CN3 superior division should have formed remains significantly wider in *Myf5*^{cre} embryos (63.96 ± 2.08 μm) than in wild-type embryos (38.26 ± 2.89 μm, $P < 0.001$) (Figs. 3J, 4B). CN3 inferior division branches to the MR and IR muscles are not visible and the branch to the IO muscle has failed to elongate (155.3 ± 87.7 μm at E14.5, 106.7 ± 44.0 μm at E15.5; Figs. 3L, 4C). This branch is significantly shorter than that in the wild type at E15.5 (477.6 ± 57.9 μm; $P < 0.001$). The CN6 trajectory remains aberrantly parallel to CN3, and its terminal axons are defasciculated (Fig. 3L, double-headed arrow).

Ocular Motor Neurons Die in the Absence of EOMs

To determine if EOMs are required for motor neuron survival, we examined the number of motor neurons in oculomotor and trochlear nuclei at E11.5 and E18.5. At E11.5, *Myf5*^{cre} and control embryos had a similar number of Isl1-positive motor neurons in the oculomotor and trochlear nuclei (4285 ± 214 control, 4477 ± 182 *Myf5*^{cre}, $P = 0.84$; Figs. 5A–C), indicating that there is normal initial proliferation of motor neurons. By E18.5, there is substantial normal developmental cell death in the control embryos, as reported previously.[7,27] *Myf5*^{cre} embryos had greater levels of cell death, however, and have significantly fewer oculomotor and trochlear neurons than control embryos (2465 ± 271 vs. 868.2 ± 81.7, $P = 0.00049$, Figs. 5D–F).

Discussion

Most prior studies of ocular cranial nerve development in mouse have relied on DiI labeling[28] or neurofilament staining,[14,16–18,29] highlighting the initial nerve trajectories but not permitting visualization of their terminal processes in the orbit. By dissecting and visualizing the mouse orbit from timed embryos with genetically labeled motor axons, we characterized in greater detail the development of mouse oculomotor, trochlear, and abducens nerves, and showed that formation of the initial nerve trajectory does not require signals from the EOMs, but formation of terminal branching does. Ocular motor nerves arrive to the orbit and form distal decision regions in a spatially and temporally similar fashion in *Myf5*^{cre} and wild-type embryos, demonstrating that axon growth and guidance from the brainstem to the proper position within the orbit is independent of EOMs and likely occurs through cues from the mesenchyme and/or through cell autonomous processes. Subsequent full nerve extension and terminal branching into the EOM targets, maintenance of correct nerve position as the orbit expands, and survival of axons and their motor neurons, however, are dependent on the presence of EOMs.

The role of EOMs in ocular motor nerve development is similar to the findings from previous reports of the contribution of skeletal muscle to spinal nerve development and survival. Silver stains and histologic sectioning following surgical ablation or irradiation of developing chick limb muscles reveal normal development of the main motor nerve trunks and distal nerve branches adjacent to the missing muscles, but failure of the formation of terminal branches that normally would innervate the missing individual muscles.[30–32] Similarly, *MyoD*$^{-/-}$::*Myf5*$^{-/-}$ mouse embryos lack all skeletal muscle and have normal initial growth and guidance of spinal motor nerves but fail to develop terminal nerve branches, followed by motor neuron apoptosis.[33] Proprioceptive sensory

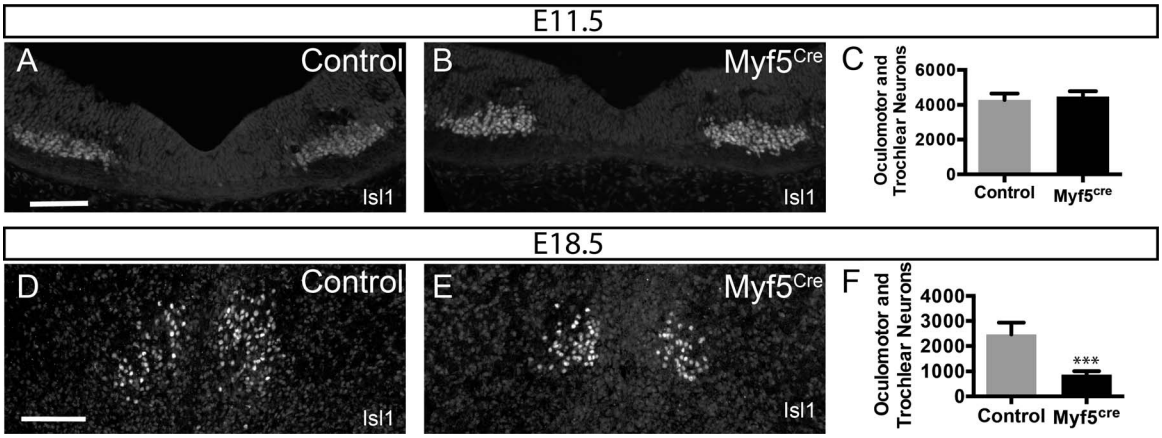

Figure 5. *Myf5^{Cre}* oculomotor and trochlear neuron number and position are similar to control at E11.5, but are significantly reduced in number by E18.5. (**A**, **B**) Oculomotor nucleus motor neurons were labeled with anti-Isl1 in control (**A**) or *Myf5^{Cre}* (**B**) brainstems at E11.5. (**C**) The number of motor neurons in the oculomotor and trochlear nuclei is equal in *Myf5^{Cre}* and control embryos at E11.5 (4285 ± 214, $n = 3$, vs. 4477 ± 182, $n = 3$, $P = 0.84$), indicating that motor neurons are formed in equal numbers. (**D**, **E**) Oculomotor nucleus motor neurons were labeled with anti-Isl1 in control (**D**) or *Myf5^{Cre}* (**E**) brainstems at E18.5. (**F**) The number of motor neurons is reduced by ~2/3 in *Myf5^{Cre}* oculomotor nucleus (2465 ± 271, $n = 3$, vs. 868.2 ± 81.7, $n = 3$, $P = 0.00049$), indicating that extraocular muscles are necessary for oculomotor neuron survival. *Scale bars*: 100 μm (**A**, **B**, **D**, **E**). *Error bars* represent SEM.

neurons are also guided by specific signals in mouse embryonic limb mesenchyme.[34] Together, these data support the influence of locally acting mesenchymal guidance cues on proximal nerve patterning and locally acting EOM cues on terminal nerve branching into target muscles.

We found minor differences in the relative timing of ocular motor nerve development in mouse compared to chick and zebrafish. In mouse we found that CN6 and CN3 reach the orbit simultaneously and before CN4, which is similar to zebrafish[21] but different from chick, in which the arrival of CN6 is followed by CN3 and then CN4.[35–37] In both mouse and chick, CN3 projects an initial nerve branch to the IO muscle, followed by branches to the MR, IR, and SR muscles.[7,35,36] By contrast, in zebrafish a branch is sent to the SR muscle many hours after branches are sent to inferior division muscles,[21] correlating with the temporal development of the CN3 nucleus, in which zebrafish SR motor neurons are born after MR and IR motor neurons.[38]

This study provided several additional insights into ocular cranial nerve development. First, we identified a trochlear branch in developing wild-type embryos that is not associated with a muscle, forms a blunt end, and subsequently retracts. Consistent with its apparent lack of muscle target, the growth and regression of this wild-type trochlear branch resembles the growth and regression of ocular nerves in *Myf5^{cre}* embryos. Future studies should better define this curious phenomenon. Second, we found that the CN3 superior division, which in the mature state forms a single branch that then divides distally to innervate both the SR and LPS muscles, fails to form in *Myf5^{cre}* embryos. This suggests that, while axons within the main trunk of CN3 are guided in a cell-autonomous manner, by axon–axon interactions, or by mesenchymal cues, the superior division axons exit from the main CN3 trunk in response to muscle cues.

We have long been puzzled by the observation that the CN3 superior division first appears as multiple small branches extending away from the main CN3 trunk, which subsequently coalesce and elongate.[7] Our current imaging approaches now reveal that, at E11.5 to E12.5, the SR/LPS muscle anlage lies in close juxtaposition to the main trunk of CN3, and these multiple small branches extend directly along and into the muscle anlage. As the orbital size expands over subsequent days, the distance between the origin and EOM targets of these small branches increases and, by E15.5, the branches have fasciculated into the superior division. *Myf5^{cre}* embryos do not form these multiple small branches, and, at the position where they normally form, the CN3 main trunk is wider than in wild-type embryos. This is reminiscent of the pathology of *Kif21a$^{KI/KI}$* mice.[7] In these mutant mice that recapitulate a human CCDD, the superior division also fails to form, and a widened bulge is visible along CN3 that, by electron microscopy, contains convoluted axon trajectories and stalled growth cones. The *Kif21a$^{KI/KI}$* bulge is located far proximally to the normal superior division branch-point and forms secondarily to attenuated Kif21a autoinhibition. By contrast, we found the *Myf5^{cre}* widening to be located at the position of the normal distal superior division branch-point. The parallels, however, suggest that the *Myf5^{cre}* nerve widening may result from paused growth cones that fail to exit the main CN3 trunk secondary to the absence of EOMs.

Ocular motor neurons, like other motor neurons, receive trophic support from their target muscles, and are responsive to neurotrophic factors, particularly BDNF[27] and GDNF[39] (see Ref. 40 for review). It is therefore not surprising that survival of ocular motor neurons depends on the presence of EOMs. It is remarkable, however, that in the absence of target muscles, more than one-third of the oculomotor and trochlear neurons remain at E18.5. By contrast, in *MyoD$^{-/-}$*::*Myf5$^{-/-}$* embryos, which lack all skeletal muscles, all somatic motor neurons in the spinal cord die by E17.5, and most motor neurons in the facial nucleus are dead or dying.[33] The ocular motor nerves are selectively spared until late in the course of motor neuron degenerative disorders such as amyotrophic lateral sclerosis and spinal motor atrophy.[41–43] This selective sparing is theorized to result from increased resistance of the ocular motor neurons to environmental stressors or excitotoxicity.[44–47] The retention of some motor neurons in CN3 and CN4 as late as E18.5 without trophic support from their target muscles may be another example of the intrinsic relative resistance of oculomotor neurons to pathologic conditions.

Using genetic tools, orbital dissection, and a developmental framework in timed mouse embryos, our findings catalogued the development of the ocular motor nerves and they implicate the EOMs in the control of their terminal branching. The identities of the signals provided by EOMs, whether they differ among different EOMs, and whether they are mediated

through short-range diffusible cues, direct contact, or both, remain to be determined.

Acknowledgments

The authors thank Michelle Delisle for mouse husbandry assistance.

Supported by the Howard Hughes Medical Institute (HHMI) Medical Research Fellows Program (SMM and JGP), the Harvard-Vision Clinical Scientist Development Program Research (5K12EY016335), the Knights Templar Eye Foundation (Career Starter Grant), the Children's Hospital Ophthalmology Foundation (Faculty Discovery Award) (MCW), and P30 HD18655 (IDDRC, Boston Children's Hospital). ECE is an HHMI investigator.

Disclosure: **S.M. Michalak**, None; **M.C. Whitman**, None; **J.G. Park**, None; **M.A. Tischfield**, None; **E.H. Nguyen**, None; **E.C. Engle**, Amgen (R)

References

1. Engle EC. The molecular basis of the congenital fibrosis syndromes. *Strabismus*. 2002;10:125–128.
2. Graeber CP, Hunter DG, Engle EC. The genetic basis of incomitant strabismus: consolidation of the current knowledge of the genetic foundations of disease. *Semin Ophthalmol*. 2013;28:427–437.
3. Nakano M, Yamada K, Fain J, et al. Homozygous mutations in ARIX(PHOX2A) result in congenital fibrosis of the extraocular muscles type 2. *Nat Genet*. 2001;29:315–320.
4. Tischfield MA, Bosley TM, Salih MA, et al. Homozygous HOXA1 mutations disrupt human brainstem, inner ear, cardiovascular and cognitive development. *Nat Genet*. 2005; 37:1035–1037.
5. Webb BD, Shaaban S, Gaspar H, et al. HOXB1 founder mutation in humans recapitulates the phenotype of Hoxb1-/- mice. *Am J Hum Genet*. 2012;91:171–179.
6. Park JG, Tischfield MA, Nugent AA, et al. Loss of MAFB function in humans and mice causes Duane syndrome, aberrant extraocular muscle innervation, and inner-ear defects. *Am J Hum Genet*. 2016;98:1220–1227.
7. Cheng L, Desai J, Miranda CJ, et al. Human CFEOM1 mutations attenuate KIF21A autoinhibition and cause oculomotor axon stalling. *Neuron*. 2014;82:334–349.
8. Miyake N, Chilton J, Psatha M, et al. Human CHN1 mutations hyperactivate alpha2-chimaerin and cause Duane's retraction syndrome. *Science*. 2008;321:839–843.
9. Tischfield MA, Baris HN, Wu C, et al. Human TUBB3 mutations perturb microtubule dynamics, kinesin interactions, and axon guidance. *Cell*. 2010;140:74–87.
10. Yamada K, Andrews C, Chan WM, et al. Heterozygous mutations of the kinesin KIF21A in congenital fibrosis of the extraocular muscles type 1 (CFEOM1). *Nat Genet*. 2003; 35:318–321.
11. Cederquist GY, Luchniak A, Tischfield MA, et al. An inherited TUBB2B mutation alters a kinesin-binding site and causes polymicrogyria, CFEOM and axon dysinnervation. *Hum Mol Genet*. 2012;21:5484–5499.
12. Nugent AA, Park JG, Wei Y, et al. Mutant α2-chimaerin signals via bidirectional ephrin pathways in Duane syndrome [published online ahead of print March 27, 2017]. *J Clin Invest*. doi:10.1172/JCI88502.
13. Kim M, Fontelonga T, Roesener AP, et al. Motor neuron cell bodies are actively positioned by Slit/Robo repulsion and Netrin/DCC attraction. *Dev Biol*. 2015;399:68–79.
14. Prakash N, Puelles E, Freude K, et al. Nkx6-1 controls the identity and fate of red nucleus and oculomotor neurons in the mouse midbrain. *Development*. 2009;136:2545–2555.
15. Lerner O, Davenport D, Patel P, Psatha M, Lieberam I, Guthrie S. Stromal cell-derived factor-1 and hepatocyte growth factor guide axon projections to the extraocular muscles. *Dev Neurobiol*. 2010;70:549–564.
16. Giger RJ, Cloutier JF, Sahay A, et al. Neuropilin-2 is required in vivo for selective axon guidance responses to secreted semaphorins. *Neuron*. 2000;25:29–41.
17. Kitsukawa T, Shimizu M, Sanbo M, et al. Neuropilin-semaphorin III/D-mediated chemorepulsive signals play a crucial role in peripheral nerve projection in mice. *Neuron*. 1997;19:995–1005.
18. Chen H, Bagri A, Zupicich JA, et al. Neuropilin-2 regulates the development of selective cranial and sensory nerves and hippocampal mossy fiber projections. *Neuron*. 2000;25:43–56.
19. Chilton JK, Guthrie S. Cranial expression of class 3 secreted semaphorins and their neuropilin receptors. *Dev Dyn*. 2003; 228:726–733.
20. Ferrario JE, Baskaran P, Clark C, et al. Axon guidance in the developing ocular motor system and Duane retraction syndrome depends on Semaphorin signaling via alpha2-chimaerin. *Proc Natl Acad Sci U S A*. 2012;109:14669–14674.
21. Clark C, Austen O, Poparic I, Guthrie S. alpha2-Chimaerin regulates a key axon guidance transition during development of the oculomotor projection. *J Neurosci*. 2013;33:16540–16551.
22. Rios AC, Marcelle C. Head muscles: aliens who came in from the cold? *Dev Cell*. 2009;16:779–780.
23. Sambasivan R, Gayraud-Morel B, Dumas G, et al. Distinct regulatory cascades govern extraocular and pharyngeal arch muscle progenitor cell fates. *Dev Cell*. 2009;16:810–821.
24. Tallquist MD, Weismann KE, Hellstrom M, Soriano P. Early myotome specification regulates PDGFA expression and axial skeleton development. *Development*. 2000;127:5059–5070.
25. Kassar-Duchossoy L, Gayraud-Morel B, Gomes D, et al. Mrf4 determines skeletal muscle identity in Myf5:Myod double-mutant mice. *Nature*. 2004;431:466–471.
26. Lewcock JW, Genoud N, Lettieri K, Pfaff SL. The ubiquitin ligase Phr1 regulates axon outgrowth through modulation of microtubule dynamics. *Neuron*. 2007;56:604–620.
27. Steljes TP, Kinoshita Y, Wheeler EF, Oppenheim RW, von Bartheld CS. Neurotrophic factor regulation of developing avian oculomotor neurons: differential effects of BDNF and GDNF. *J Neurobiol*. 1999;41:295–315.
28. Fritzsch B, Nichols DH, Echelard Y, McMahon AP. Development of midbrain and anterior hindbrain ocular motoneurons in normal and Wnt-1 knockout mice. *J Neurobiol*. 1995;27: 457–469.
29. Mar L, Rivkin E, Kim DY, Yu JY, Cordes SP. A genetic screen for mutations that affect cranial nerve development in the mouse. *J Neurosci*. 2005;25:11787–11795.
30. Lewis J, Chevallier A, Kieny M, Wolpert L. Muscle nerve branches do not develop in chick wings devoid of muscle. *J Embryol Exp Morphol*. 1981;64:211–232.
31. Phelan KA, Hollyday M. Axon guidance in muscleless chick wings: the role of muscle cells in motoneuronal pathway selection and muscle nerve formation. *J Neurosci*. 1990;10: 2699–2716.
32. Tosney KW, Landmesser LT. Growth cone morphology and trajectory in the lumbosacral region of the chick embryo. *J Neurosci*. 1985;5:2345–2358.
33. Kablar B, Rudnicki MA. Development in the absence of skeletal muscle results in the sequential ablation of motor neurons from the spinal cord to the brain. *Dev Biol*. 1999; 208:93–109.
34. Poliak S, Norovich AL, Yamagata M, Sanes JR, Jessell TM. Muscle-type identity of proprioceptors specified by spatially

restricted signals from limb mesenchyme. *Cell*. 2016;164:512–525.

35. Chilton JK, Guthrie S. Development of oculomotor axon projections in the chick embryo. *J Comp Neurol*. 2004;472:308–317.
36. Hasan KB, Agarwala S, Ragsdale CW. PHOX2A regulation of oculomotor complex nucleogenesis. *Development*. 2010;137:1205–1213.
37. Wahl CM, Noden DM, Baker R. Developmental relations between sixth nerve motor neurons and their targets in the chick embryo. *Dev Dyn*. 1994;201:191–202.
38. Greaney MR, Privorotskiy AE, D'Elia KP, Schoppik D. Extraocular motoneuron pools develop along a dorsoventral axis in zebrafish, Danio rerio. *J Comp Neurol*. 2017;525:65–78.
39. Chen J, Butowt R, Rind HB, von Bartheld CS. GDNF increases the survival of developing oculomotor neurons through a target-derived mechanism. *Mol Cell Neurosci*. 2003;24:41–56.
40. Benitez-Temino B, Davis-Lopez de Carrizosa MA, Morcuende S, Matarredona ER, de la Cruz RR, Pastor AM. Functional diversity of neurotrophin actions on the oculomotor system. *Int J Mol Sci*. 2016;17:E2016.
41. Comley LH, Nijssen J, Frost-Nylen J, Hedlund E. Cross-disease comparison of amyotrophic lateral sclerosis and spinal muscular atrophy reveals conservation of selective vulnerability but differential neuromuscular junction pathology. *J Comp Neurol*. 2016;524:1424–1442.
42. Leveille A, Kiernan J, Goodwin JA, Antel J. Eye movements in amyotrophic lateral sclerosis. *Arch Neurol*. 1982;39:684–686.
43. Sharma R, Hicks S, Berna CM, Kennard C, Talbot K, Turner MR. Oculomotor dysfunction in amyotrophic lateral sclerosis: a comprehensive review. *Arch Neurol*. 2011;68:857–861.
44. Haenggeli C, Kato AC. Differential vulnerability of cranial motoneurons in mouse models with motor neuron degeneration. *Neurosci Lett*. 2002;335:39–43.
45. Brockington A, Ning K, Heath PR, et al. Unravelling the enigma of selective vulnerability in neurodegeneration: motor neurons resistant to degeneration in ALS show distinct gene expression characteristics and decreased susceptibility to excitotoxicity. *Acta Neuropathol*. 2013;125:95–109.
46. Hedlund E, Karlsson M, Osborn T, Ludwig W, Isacson O. Global gene expression profiling of somatic motor neuron populations with different vulnerability identify molecules and pathways of degeneration and protection. *Brain*. 2010;133:2313–2330.
47. Lorenzo LE, Barbe A, Portalier P, Fritschy JM, Bras H. Differential expression of GABAA and glycine receptors in ALS-resistant vs. ALS-vulnerable motoneurons: possible implications for selective vulnerability of motoneurons. *Eur J Neurosci*. 2006;23:3161–3170.

Investigative Ophthalmology & Visual Science